Powder Technology xxx (2019) xxx

Contents lists available at ScienceDirect

Powder Technology

journal homepage: www.elsevier.com/locate/powtec

Investigation of continuous carbothermal reduction of magnesia by magnesium vapor condensation onto a moving bed of solid particles

Boris A. Chubukov [a], Scott C. Rowe [a], Aaron W. Palumbo [a,b], Mark A. Wallace [a,b], Alan W. Weimer [a,*]

[a] Department of Chemical and Biological Engineering, University of Colorado Boulder, 596 UCB, Boulder, CO 80309-0596, USA
[b] Big Blue Technologies LLC, 6710 W 112th PL, Westminster, CO 80020, USA

ARTICLE INFO

Article history:
Received 22 May 2018
Received in revised form 1 November 2018
Accepted 24 January 2019
Available online xxxx

Keywords:
Kinetics
Process engineering
Moving bed
Smelting
Gasification
Magnesium

ABSTRACT

Magnesium metal production by carbothermic reduction (CTR) can reduce process emissions and energy requirements relative to silicothermic or electrolytic production, if high magnesium metal yields are achieved. A novel process was investigated where product magnesium gas condensed onto a moving bed of solid particles at high temperatures (≥300 °C) and in vacuum to minimize reversion and promote crystal growth. Using a half-system in which CTR product gases were artificially generated, magnesium continuously condensed onto steel, oxide, or carbide particles at yields >85% for $P_{Mg} = 0.5$ kPa. Steel particles exhibited the greatest bed retention and ease of separation, so this medium was used for scale-up to a full-system in which MgO CTR in a fixed bed gasifier at 1400 °C–1550 °C produced $Mg_{(g)}$ and CO. The initial reduction resulted in high Mg yield (>80%), but yield decreased as the reaction proceeded. The accumulation of $Mg_{(s)}$ and reversion product in the condenser promoted further reversion. The process yield could likely be improved by using high surface area particles to promote heat and mass transfer, allowing for shorter solid and gas residence times in the condenser. A finite volume model on the reactor tube and pellet bed described the kinetics, heat transfer, and mass transfer phenomena in the reduction reactor. The model predicted that the center of the bed was >50 °C cooler than the furnace, and the product gas pressures were near equilibrium. A wide and directly heated reactor could overcome these heat and mass transfer limitations.

1. Introduction

Carbothermic reduction (CTR) of magnesium oxide can be an economic and clean alternative to primary magnesium production over electrolytic or silicothermic production [1]. The large energy input for electrolytic (174 MJ/kg Mg) and silicothermic production (287 MJ/kg Mg) result in high production costs: $3.11 and $2.44–$2.88/kg, respectively [2,3]. Using coal as the main energy source lowers the production costs for silicothermic production, but this results in large emissions (37–47 kg CO_2-eq/kg Mg) relative to electrolytic production (20–26 kg CO_2-eq/kg Mg) [2]. Production by carbothermal reduction can be a cheaper ($1.83/kg Mg) method because of reduced energy requirements (43 MJ/kg Mg) and capital costs [3]. The lower energy requirement should reduce process emissions.

At the temperature required for carbothermal reduction, reaction (1), magnesium metal is liberated as a gas.

$$MgO + C \leftrightarrow Mg_{(g)} + CO \quad (1)$$

The effective condensation of $Mg_{(g)}$ has proven difficult because CO and $Mg_{(g)}$ readily revert to C and MgO. Many attempts [4–24] have been made in the last 100 years to achieve high metal yield from MgO CTR. Notably, three commercial plants were established, surrounding wartime efforts during WWII, operating on the principle of quenching by inert gas dilution. The hot stream of CO and $Mg_{(g)}$ was diluted by cool hydrogen or natural gas to a stable temperature (~200 °C [5]) below which reversion did not occur, and $Mg_{(g)}$ condensed homogeneously. The product was a fine and impure powder (Mg, MgO, C) requiring vacuum distillation for purification. Low yields from condensation (~50% [7]), difficulties in collecting and briquetting the pyrophoric powder product, and the energy and labor intensity of vacuum distillation prevent that process from being profitable today.

More recently, the Magsonic process [8] demonstrated >90% yield of Mg by gas quenching using a laval nozzle, and Winand et al. [4] demonstrated 80% yield of Mg by condensing on solid surfaces with scrapers, however, the overall ore-to-ingot yield was not reported and neither process has been commercialized.

Other condensation methods include condensing within the gas phase [8,9,21,24], into a suitable liquid [6,11,12,15,17,22], and onto a solid surface [4,13,14,18,19,23,25]. Despite these efforts, no commercial process exists for magnesium production by carbothermal reduction.

* Corresponding author.
E-mail address: alan.weimer@colorado.edu (A.W. Weimer).

https://doi.org/10.1016/j.powtec.2019.01.067
0032-5910/

Unfortunately, the results of the majority of these projects are not publically documented. It is likely that reversion, separation, and purification were the primary reasons for failure. A tremendous opportunity exists if one can overcome these challenges.

Under high temperature (>300 °C) and vacuum conditions, $Mg_{(g)}$ from MgO CTR condenses heterogeneously to produce large Mg grains (>1 mm) at high yields (>95%) [26–29]. Magnesium condensate of this size is less susceptible to oxidation in air and may be purified by melting. The challenge remains in effectively removing product magnesium from the condenser. Here, product magnesium condensed onto solid particles (condensation media) that flowed as a moving bed. To investigate the feasibility of such operation, an artificial mixture of $Mg_{(g)}$ and CO impinged onto a perpendicular stream of condensation media flowing downward with gravity. Results from this half-system guided the scale-up of the condenser for use in the full-system. There, equimolar C/MgO pellets in a fixed bed gasifier generated $Mg_{(g)}$ and CO to feed into the condenser. Product $Mg_{(s)}$ was collected and purification was attempted by melting and vacuum distillation.

2. Methods

2.1. Half-system for $Mg_{(g)}$ condensation

Fig. 1 depicts both experimental systems used in this study. The half-system, Fig. 1a, reproduced MgO CTR product gases by evaporating $Mg_{(s)}$ and mixing with CO (equimolar). This mixture impinged onto cooler condensation media flowing with gravity in a cross flow. Magnesium condensed onto the media, and both solids were removed together. The system resembled a heat exchanger wherein the condensation media absorbed the latent heat of magnesium condensation, the sensible heat of the gas stream, and the heat of the reversion reaction. The effect of inlet solids temperature, condensation medium, and $Mg_{(g)}$ partial pressure on bed retention and $Mg_{(s)}$ yield were investigated.

The half-system was constructed entirely of 5.08 cm OD and 4.76 ID stainless steel (SS, 304/316) tubing. Nichrome heaters and K-type thermocouples on the external tubing maintained wall temperatures. Stainless steel foil (50 μm thick) lined the inner tubing to collect $Mg_{(s)}$/MgO/C deposits. A vacuum pump (Adixen ACP 40), pressure sensors (MKS 626B), and butterfly throttle valve (MKS T3BI) controlled vacuum within the system. Stainless steel mesh (0.86 mm openings) prevented the media from flowing into the horizontal arms of the system. A multi-probe thermocouple (Omega) along the centerline of the solids flow measured the temperature profile in the condenser. Heaters surrounding the tubing above the condensation zone preheated the media, and the inlet solids temperature into the condensation zone could be controlled by altering the bed velocity and/or the wall temperature in the preheating zone. An auger (Hapman X07423SD-A50) controlled the solids flow rate, and a stepper motor (SureStep STP-MTRH-34066) drove the auger rotation through a rotary vacuum feedthrough (Pfeiffer D-35614). One hopper supplied fresh material at the top of the condenser, and a second hopper collected the product below. A laser (Dimetix FLS—C30) mounted on the feed hopper measured the level and flow rate of solids. Mass flow controllers (MKS) fed Ar and CO gas into the system. A gas analyzer (NOVA 7905 AH) downstream of the pump measured the concentrations of CO, CO_2, and CH_4 by infra-red absorption, O_2 by electrochemical detection, and H_2 by thermal conductivity change.

2.2. Half-system operating procedure

Ten grams of magnesium (American Elements, 99.9%, 1–10 mm) were loaded into an alumina crucible, and the crucible was pushed into the horizontal tubing upstream of the condensation area. The walls surrounding this area were preheated to 300 °C as the rest of the system was brought to temperature. Carbon monoxide was fed through a long and narrow tube (OD = 3.175 mm) that extended from the vacuum flange over the magnesium metal pieces. A flow of Ar (0.5 slm)

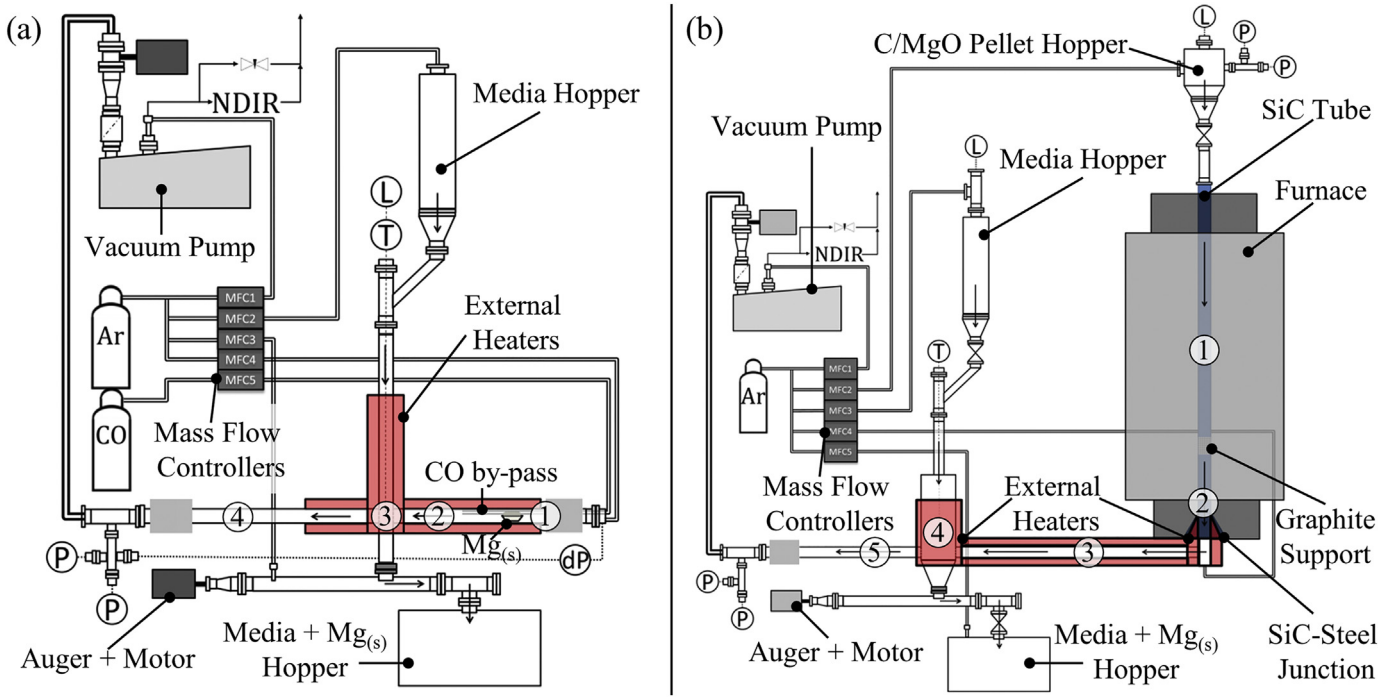

Fig. 1. Measurements are "L" = level, "P" = pressure, "T" = temperature, "dP" = pressure differential. (a) Half-system: $Mg_{(s)}$ evaporated in vacuum at 725 °C (1) produced $Mg_{(g)}$. CO fed downstream of the evaporating zone mixed with $Mg_{(g)}$ at 850 °C (2) and flowed into a moving bed of media (3), where $Mg_{(g)}$ deposited. CO passes through the moving bed by pumping, and the remainder of $Mg_{(g)}$ deposited on the outlet walls (4). (b) Full-system: Equimolar C/MgO pellets gasified in a vacuum furnace at ≥1400 °C (1). Product gases traveled through a water-cooled seal (2), through a transfer line (3), and impinged onto steel media in a moving bed condenser (4). CO passes through the moving bed by pumping, and the remainder of $Mg_{(g)}$ deposited on the outlet walls (5).

Please cite this article as: B.A. Chubukov, S.C. Rowe, A.W. Palumbo, et al., Investigation of continuous carbothermal reduction of magnesia by magnesium vapor condensation onto ..., Powder Technol., https://doi.org/10.1016/j.powtec.2019.01.067

over the crucible and $Mg_{(s)}$ prevented backflow of CO and $Mg_{(g)}$. The walls of the vertical tubing above the condensation zone were heated to between 150 °C and 550 °C, while the auger removed solids from the condenser at a velocity between 0.1 and 2.0 m/h. The wall of the horizontal tubing at the cross inlet and outlet were heat to 750 °C to prevent any blockage there. The pressure in the system was varied between 1.5 and 10 kPa, corresponding to $Mg_{(g)}$ partial pressures between 0.5 and 2.2 kPa. Once steady-state temperatures were reached in the moving bed condenser, the area surrounding the magnesium metal pieces was raised to 725 °C within 10 min. The wall temperature at the point of $Mg_{(g)}$ and CO mixing was maintained at 850 °C. No deposits were observed in this region. After a ~5 min start-up period, the evaporation rate of $Mg_{(s)}$ became fairly constant, 29.96 ± 0.13 g/h, relating to a CO flow of 0.46 slm. This evaporation rate was determined by linear regression of $Mg_{(s)}$ weight loss from the crucible for several heating times. Steady-state conditions were maintained for 15–20 min. The depletion of magnesium pieces from the alumina boat was detected by the decrease in energy input into the heaters surrounding this zone.

Half-system yield (Y_{hs}) of $Mg_{(s)}$ from $Mg_{(g)}$ was estimated based on the decrease in CO concentration in the effluent.

$$Y_{hs}(t) = 1 - \frac{\dot{n}_{CO,Initial} - \dot{n}_{CO}}{\dot{n}_{Mg,evaporation}} \tag{2}$$

Based on the measured Mg evaporation rate and the accuracy of the instrumentation used, the standard measurement error of the half-system yield was approximately ±3.9%. Some of the vaporized magnesium passed through the condensation media and condensed downstream of the moving bed. Bed retention (R_B) was defined as the fraction of magnesium that condensed within the bed. This was estimated by the mass and purity of the condensate downstream of the bed.

$$R_B = 1 - \frac{m_{Mg,downstream}}{m_{Mg,vaporized}} \tag{3}$$

Condensation media used for testing are described in Table 1. Condensed magnesium was separated from the media by vacuum distillation in a SiC (hexoloy) crucible at 750 °C and 1 kPa. This formed a crown of Mg on the walls of the crucible.

2.3. Full-system for continuous MgO CTR and $Mg_{(g)}$ condensation

The full-system, Fig. 1b, generated $Mg_{(g)}$ and CO by carbothermal reduction of equimolar C/MgO pellets within a SiC (Hexoloy) tube (5.08 cm OD, 3.81 ID, 2.0 m long). To form pellets, petcoke and magnesia were milled together for 15 min in an HD-01 attritor from Union Process, and the resulting powder was extruded through a 3.0 mm die using a D150G pelletizer (13 HP). Oil lubricated the flow of material through the die, and a blade at the end of the die cut extrusions to 12 mm. These pellets were pyrolyzed in N_2 at 650 °C prior to loading into the reduction furnace.

Pellets in the reduction furnace gasified upon reaction, and the bed collapsed. A laser measured the reduction in bed height. A hopper above the SiC tube provided a constant supply of fresh pellets into the reduction zone. A porous graphite pedestal maintained the bottom of the bed 17.8 cm above the bottom of the hot-zone. Product $Mg_{(g)}$ and CO flowed out the bottom of the SiC tube, through a water-cooled connection to SS tubing, through a 4.76 cm ID SS (304/316) transfer tube (60.96 cm long), and into a 14.91 ID moving bed condenser. The bottom of the SiC tube was flared from 5.08 cm OD to 15.24 cm OD which mated to a SS cone of the same geometry. Thus, the internal gas pathway remained hot and unperturbed, while an effective cooling fin was created by the flared ends, allowing for a water-cooled o-ring seal there. Nichrome heaters lining the outside of all tubing connecting the furnace to condenser maintained the temperature of the gas stream at ≥850 °C to prevent condensation and reversion there. In the condenser, MgO CTR product gases impinged onto steel (SS 440c, 3.125 mm) media flowing downward with gravity. The inlet and outlet of the condenser (4.76 cm ID) were across from one another. Ar flow from the top and bottom of the reacting bed and moving bed condenser maintained the gas path. Pressure sensors and relief valves were mounted upstream of the reacting bed and downstream of the condenser. A 38 kW split furnace from CM (1735–36 VT) with $MoSi_2$ heating elements and three independently controlled temperature zones provided the heat for the reduction. The heated zone extended vertically 91.44 cm. Vacuum control, level measurement, gas flow, and gas analysis were setup using the same instruments as in the half-system.

Table 1
Condensation media tested in half-system.

Vendor	Material	Size [mm]
Saint-Gobain	SiO_2/ZrO_2 (oxide)	2.0–2.5
Fox Industries	440c SS (steel)	3.1
Gallium Source	Mg	1.5–2.0
Industrial Filter	Activated Carbon	4.0
Kramer Industries	SiC grit (carbide)	2.0–2.3

2.4. Full-system operating procedure

The SiC tube was filled to the top (1.4–1.5 kg pellets), and the condenser feed hopper was filled with 45–50 kg of media. After sealing, the system was pre-heated under vacuum (condenser to 300 °C, transfer tube to 500 °C, furnace to 650 °C) for 12 h to remove any moisture. After degassing, the transfer tube temperature was raised to 850 °C and the furnace temperature was raised to the operating temperature (10 °C/min for $T < 1000$ °C, 5 °C/min for $T > 1000$ °C). Once the furnace reached 1000 °C, the media flow was initiated, and the wall temperature surrounding the condensation zone was raised to 750 °C. The ratio of $\dot{m}_{Media} : \dot{m}_{Mg}$ was maintained at 200:1. This resulted in an inlet solids temperature near 300 °C into the condensation zone. The final furnace temperature was varied between 1400 °C and 1550 °C, and the outlet pressure of the condenser was fixed at 1.0 kPa.

Magnesium metal production was estimated by the decrease in bed height during reduction. This value agreed well with the overall mass balance before and after reduction. The full-system yield (Y_{fs}) of magnesium metal was estimated by comparing the production rate to the CO emission during reduction.

$$Y_{fs}(t) = \frac{\dot{n}_{CO}(t)}{C_{MgO} A_z \vec{v}_{z,bed}} \tag{4}$$

The production rate of $Mg_{(g)}$ was fairly constant ($\pm 1.3 \cdot 10^{-5}$ mol/s) during reduction. Based on this value and the accuracy of the instrumentation used, the standard measurement error of the full-system yield was approximately ±0.62%. The reactor was operated at a pseudo-steady-state for up to 3.5 h, after which the system was cooled to room temperature. Product magnesium and condensation media were separated by mechanical sieving and/or by vacuum distillation in a steel retort (14.61 cm ID, 1.2 m long). The distillate was melted and poured into an ingot. Melting of product Mg was in a graphite crucible with M134 flux (SRC) and/or SF_6 cover-gas. Care was taken when handling any magnesium product.

2.5. Material characterization

Anode grade petcoke obtained from Marathon Petroleum in the form of 0.5–10 cm agglomerates served as the reductant. Magnesium oxide obtained from Premier Magnesia in the form of a high surface area (147 m^2/g) powder served as the ore source. The compositions of the raw feedstock are listed in Table 2. In pellets, carbon and oxygen

Please cite this article as: B.A. Chubukov, S.C. Rowe, A.W. Palumbo, et al., Investigation of continuous carbothermal reduction of magnesia by magnesium vapor condensation onto ..., Powder Technol., https://doi.org/10.1016/j.powtec.2019.01.067

Table 2
Composition of carbon and magnesium oxide sources.

	Metals (ppm)					Non-metals (wt%)	
Materials	Ca	Si	Fe	Ni	V	S	Volatiles
Petcoke	170	45	210	250	710	4.7	11
Magnesia	6100	1600	900	<10	<10	<0.01	4.5

elemental compositions were determined by oxidation in O_2 using a LECO C200 and reduction by C using a LECO TC600, respectively. Magnesium oxide content was estimated assuming all oxygen was bound as magnesium oxide. Imaging was performed by field emission scanning electron microscopy (FESEM) using a JEOL 7401 F microscope equipped with energy dispersive x-ray spectroscopy (EDS). Thermal diffusivity of pellets was measured by laser flash analysis (LFA) using a Netzsch LFA 457.

3. Results & discussion

3.1. Theoretical considerations for a moving bed condenser

The principle of operation requires that the solid phase absorb the latent heat of magnesium condensation, the sensible heat of the gas stream, and the heat of the reversion reaction. In this sense, the system can be treated as an adiabatic heat exchanger. An overall energy balance on the system is:

$$\begin{aligned}\dot{m}_s Cp_s(T_{s,f}-T_{s,i}) = {} & \dot{m}_{Ar}Cp_{Ar}(T_{g,i}-T_{g,f}) + \dot{m}_{CO}Cp_{CO}(T_{g,i}-T_{g,f}) \\ & + \dot{m}_{Mg}Cp_{Mg_{(g)}}(T_{g,i}-T_{cond}) \\ & + \dot{m}_{Mg}Cp_{Mg_{(l)}}(T_{cond}-T_{frez}) \\ & + \dot{m}_{Mg}Cp_{Mg_{(s)}}(T_{frez}-T_{s,f}) + \dot{m}_{Mg}\Delta H_{cond} \\ & + \dot{m}_{Mg}\Delta H_{frez} + \dot{m}_{Mg}\Delta H_{r1}(1-Y) \end{aligned} \quad (5)$$

assuming that reversion occurs at the final solids temperature ($T_{s,f}$). The latent heat of condensation and freezing, $\Delta H_{cond}^{650°C} + \Delta H_{frez}^{650°C} = 141$ *kJ/mol*, and the heat of reversion, $\Delta H_{r1}^{500°C} = 634$ *kJ/mol*, can dominate the right-hand side of the equation. Given 90% yield of $Mg_{(s)}$ from $Mg_{(g)}$, condensation and freezing at 650 °C, an inlet gas temperature ($T_{g,i}$) of 1000 °C, and an outlet gas ($T_{g,f}$) and solids ($T_{s,f}$) temperature of 500 °C, the heat of condensation and heat of reversion make up 89.9% of the total heat released. Given that the condensation media heats up 300 °C, the minimum media to magnesium mass flow ratio, $\dot{m}_s : \dot{m}_{Mg}$, is 60:1. This value served as a baseline for the mass flow rate of solids. A volume balance under these conditions predicts that 3.73% of the bed volume (random packing) is taken up by condensate.

The larger the temperature increase of the condensation medium, the lower the theoretical $\dot{m}_s : \dot{m}_{Mg}$ ratio. If the inlet temperature of the condensation medium is too low, shock-cooling (high Mg supersaturation) results in extremely fine Mg particles susceptible to oxidation by CO or air (when the reactor is opened). A higher initial inlet temperature promotes Mg condensation into large particles and minimizes reversion. Thus a balance exists between a low inlet temperature (large potential temperature increase, more reversion) and a higher inlet temperature (lower potential temperature increase, less reversion). The chosen values represent a balance of these two phenomena.

3.2. Experimental results for half-system

The half-system allowed for controlled testing of the principle of operation. The effect of inlet solids temperature, condensation medium, and $Mg_{(g)}$ partial pressure on bed retention (R_B) and yield (Y_{hs}) were analyzed, to determine conditions for full-system operation. The ratio of $\dot{m}_s : \dot{m}_{Mg} = 150{:}1$ was used for these experiments.

No deposition occurred in the area of $Mg_{(g)}$ and CO mixing (850 °C). The metastability of a $Mg_{(g)}$ and CO mixture was again [27,30] observed here. The gas mixture was well below the temperature at which reversion is thermodynamically favored, but no reversion occurred. The absence of condensation on the inlet side SS mesh and on the wall of the condensation zone (750 °C) allowed for clog-free operation. The moving bed did not reach the wall temperature which allowed for condensation on the media. Some $Mg_{(g)}$ passed through the moving bed and condensed downstream of the condensation zone.

Using activated carbon particles as condensation media resulted in extreme reversion ($Y = 32.6 \pm 1.0\%$). Moisture within the carbon reacted with $Mg_{(g)}$, as H_2 was observed in the effluent. Based on the integration of the H_2 signal, 16% of the total extent of reversion occurred from reaction with moisture, suggesting that either fine MgO formed from reaction with moisture or the carbon particles themselves served as nucleation sites for further reversion, accelerating the reversion rate. Despite efforts to pre-heat and degas this media, the yield was not improved. Magnesium particles as condensation media reacted with CO during pre-heating, and the solid phase froze from particle sintering. Reversion occurred between $Mg_{(s)}$ and CO at 300 °C but not between $Mg_{(g)}$ and CO at 850 °C. Any condensed magnesium must be quickly removed from the system. Magnesium condensed onto oxide, steel, and carbide media at high yields (>85%) and without bed clogging. Images of Mg condensate on these media are shown in Fig. 2. Relatively little condensation occurred on carbide media, and no large particles of Mg were visible. Reversion product, C and MgO, were seen as particles on the carbide surface, and Mg was detected on the carbide surface by EDS. On oxide media, Mg globules and reversion product were seen on the surface. On steel medium, large Mg particles and reversion product were seen on the surface.

The temperature at the center of the condensation zone increased up to 82 °C during the condensation. The concentration of CO initially decreased upon $Mg_{(s)}$ evaporation and reached a fairly constant level for 15–20 min until all $Mg_{(s)}$ had evaporated. Fig. 3 shows that, when

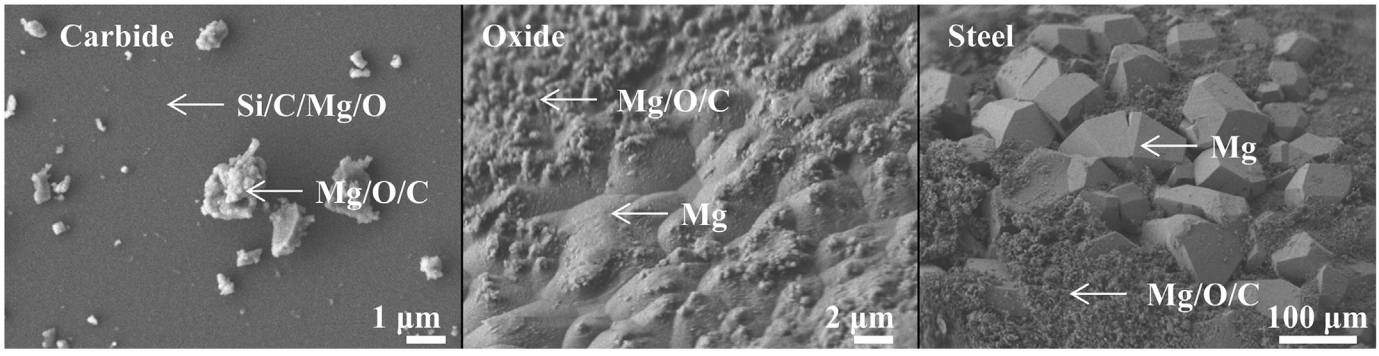

Fig. 2. SEM images of Mg condensate on carbide, oxide, and steel medium from $Mg_{(g)}$ condensation in the half-system at an inlet solids temperature of 475 °C and $P_{Mg} = 0.5$ kPa. Elemental labeling was based on those elements observed by EDS at the indicated arrow position.

Please cite this article as: B.A. Chubukov, S.C. Rowe, A.W. Palumbo, et al., Investigation of continuous carbothermal reduction of magnesia by magnesium vapor condensation onto ..., Powder Technol., https://doi.org/10.1016/j.powtec.2019.01.067

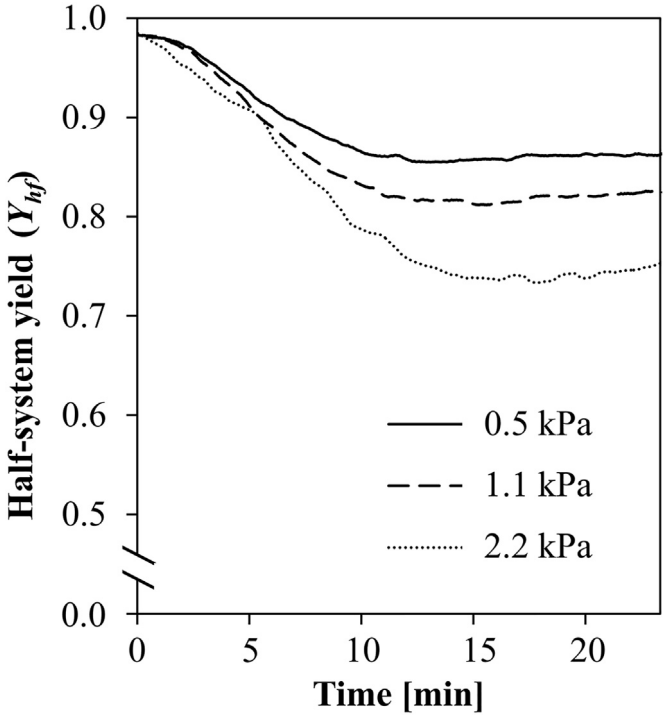

Fig. 3. Yield of $Mg_{(s)}$ from $Mg_{(g)}$ during operation of half-system given the indicated CO and $Mg_{(g)}$ partial pressures using steel media at an inlet solids temperature of 342 °C.

using steel media, the extent of reversion increased with $Mg_{(g)}$ and CO partial pressures, as has been previously documented [26,27]. The appearance of a steady-state suggested that continuous condensation at high yields is achievable in a moving bed condenser.

Bed retention increased with decreasing T_{s_i} between 300 °C and 625 °C, Fig. 4, suggesting that condensation was limited by heat transfer within this temperature range. Magnesium condensed more readily onto steel media than oxide media, likely because of its relatively high thermal conductivity, however magnesium did not readily condense onto carbide media despite its high thermal conductivity. As molten magnesium has a relatively low contact angle on silicon carbide [31,32], it is possible that film condensation occurred on carbide media while dropwise condensation occurred on steel and oxide media. Dropwise condensation can lead to higher heat transfer rates than film condensation, thus, even though the carbide media had the highest intrinsic thermal conductivity, an Mg film could have hindered further condensation resulting in the relatively low bed retention.

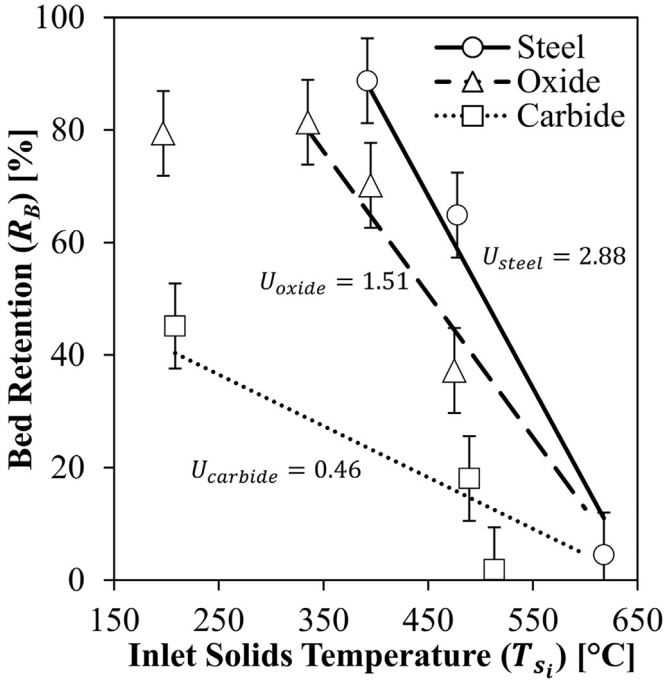

Fig. 4. Effect of inlet solids temperature on bed retention for steel, oxide, and carbide media for P_{Mg} = 0.5 kPa. Points show experimental values and lines show theoretical prediction. The fitted heat transfer coefficient (U) is listed in [$W \cdot m^{-2} \cdot K^{-1}$].

Condensed magnesium volatilized from steel media during vacuum distillation but reacted with oxide media. No magnesium was recovered from oxide media. Steel media was selected for full-system operation. These experiments on the half-system suggest that high thermal conductivity and poor Mg wetting of the media promotes high heat transfer and condensation rates. As carbide, oxide, and steel media were all fully densified they had a similar specific surface area, so the effect of surface area could not be determined. Further investigation is necessary truly determine the best condensation media.

An overall heat transfer coefficient, based on the rate of heat exchange, quantified the effectiveness of each media, Eq. (6), and Fig. 4 illustrates the model fits for carbide, oxide, and steel media at inlet solid temperatures between 300 °C and 625 °C.

$$\dot{Q} = UA\Delta T_{LM} \tag{6}$$

The condenser used in the half-system was 4.76 cm ID and did not achieve complete bed retention for $\dot{m}_{Mg} = 29.96 \pm 0.13$ g/h. To achieve complete bed retention in the full-system, $\dot{m}_{Mg} > 100$ g/h, the condenser was scaled-up. Calculations based on the overall heat transfer coefficient predicted that a 14.91 cm ID condenser would achieve complete bed retention given $T_{s_i} < 400$ °C and $\dot{m}_s/\dot{m}_{Mg} = 200$.

3.3. Experimental results for full-system

Operation of the half-system demonstrated the technical feasibility of the process. The full-system expanded on these results by scaling up the production rate ($\dot{m}_{Mg}$>100 g/h) and generating $Mg_{(g)}$ from MgO CTR.

The full-system was operated at furnace temperatures from 1400 °C to 1550 °C and at a constant condenser outlet pressure of 1.0 kPa. The pressure drop across the condenser increased from 0.1 kPa to 1.1 kPa with increasing furnace temperature. Fig. 5 shows representative samples from each area of the reactor. No products or residue deposited within the hot zone (1) of the furnace. Silicon and sulfur impurities and carbon and magnesium oxide from reversion deposited immediately below the hot zone (2). These hard deposits were difficult to remove and accounted for 3.7 ± 1.1% of the total deposits. A similar amount (2.0 ± 1.9%) condensed inside the transfer tube (3), but as the transfer tube was much longer (60.96 cm) than the length of deposits below the hot zone (15.24 cm), these deposits were more dispersed. Carbon dioxide and other oxide impurities (SO_x, SiO) likely caused reversion and deposition below the hot zone (2) because they react readily with $Mg_{(g)}$. After these volatile oxides reacted, relatively little condensation occurred along the transfer tube (3) because of the metastability of CO and $Mg_{(g)}$. Further, silicon and sulfur impurities present below the hot zone (2) were not observed in the transfer tube (3). The majority of condensation (92.1 ± 3.1%) occurred within the condenser (4), and a significant amount (2.9 ± 1.6%) of condensation occurred downstream of the condenser (5). In the condenser, magnesium condensed onto the media but was also present as a powder (63.3 ± 0.9% Mg). Downstream of the condenser, magnesium deposited as an impure powder (47.9 ± 3.9% Mg).

Please cite this article as: B.A. Chubukov, S.C. Rowe, A.W. Palumbo, et al., Investigation of continuous carbothermal reduction of magnesia by magnesium vapor condensation onto ..., Powder Technol., https://doi.org/10.1016/j.powtec.2019.01.067

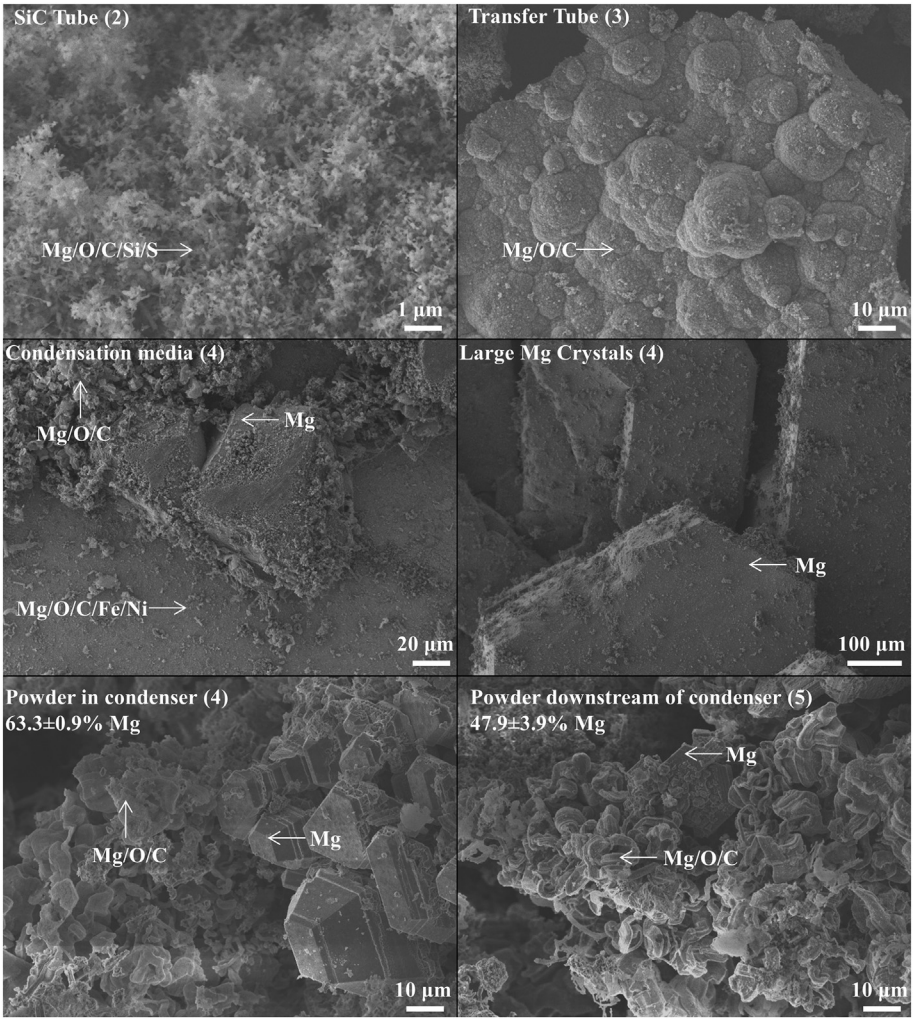

Fig. 5. Representative deposits collected from the full-system after reduction at 1400 °C for 2.5 h. Numbering corresponds to areas of the full-system as described in Fig. 1b. Elemental labeling was based on those elements observed by EDS at the indicated arrow position.

Fig. 6a illustrates that the reduction rate increased from 12.5 ± 5.3 g/h Mg to 115.1 ± 5.3 g/h Mg from 1400 °C to 1550 °C. Fig. 6b shows that the instantaneous yield within the condenser, based on Eq. (4), decreased over time. The initial condensation onto a solid surface resulted in a high yield of $Mg_{(s)}$ from $Mg_{(g)}$, but further condensation promoted reversion. Hansgirg [5] previously attributed this phenomenon to poor heat transfer through the product layer; however, this phenomenon was not observed in the half-system, and the product

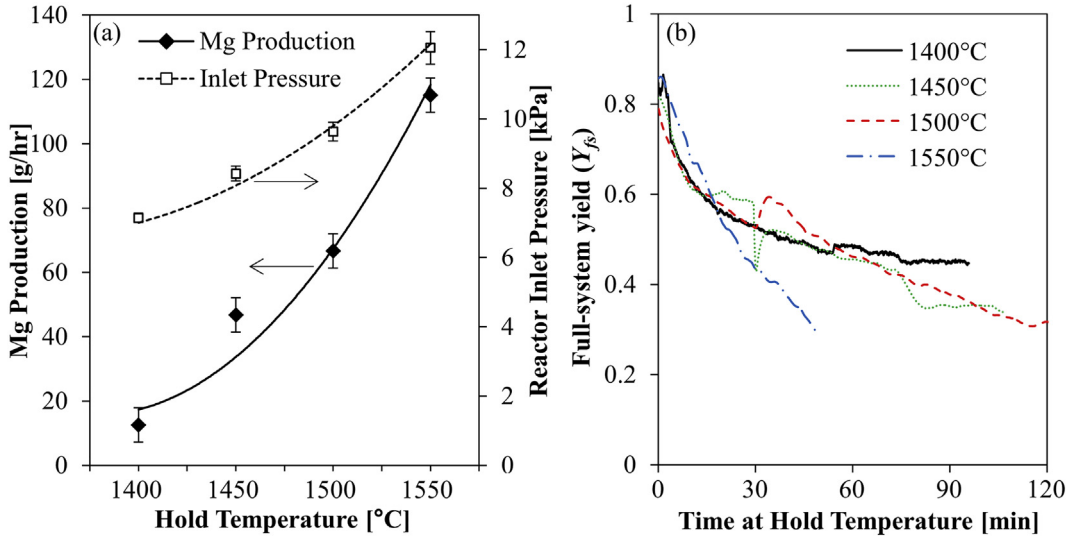

Fig. 6. (a) Pseudo-steady-state magnesium production rate and reactor pressure with furnace temperature and (b) non-steady-state yield of $Mg_{(s)}$ from $Mg_{(g)}$ during reduction.

Please cite this article as: B.A. Chubukov, S.C. Rowe, A.W. Palumbo, et al., Investigation of continuous carbothermal reduction of magnesia by magnesium vapor condensation onto ..., Powder Technol., https://doi.org/10.1016/j.powtec.2019.01.067

layer on the media in the full-systems should have been thinner than that of the half-system as $\dot{m}_s : \dot{m}_{Mg_{(g)}}$ was increased from 150:1 (half-system) to 200:1 (full-system). In the half-system condenser, the residence time of gases and solids, estimated based on the volumetric flows and internal cross volume, was shorter than that in the full-system ($\tau_{solids} = 170\ s \rightarrow 340\ s$, $\tau_{gases} = 8.0\ ms \rightarrow 16\ ms$). This increase in residence time may have promoted reversion because condensed magnesium remained in a CO stream at high temperature (>300 °C) for a prolonged period of time. Further, reversion product can act as a nucleation point for further reversion, speeding up the reversion rate [33], so the accumulation of reversion product within the condenser may have promoted further reversion. The high initial yield (>80%) may be maintained by reducing the gas and solids residence times. This could be achieved by using a higher surface area medium to promote heat and mass transfer, allowing for a shorter residence time while maintaining high bed retention.

Magnesium condensate showed large crystalline regions, likely the result of initial high-yield condensation, and finer Mg/MgO/C powders, likely the result of further low-yield condensation. Some of the condensate (~1/3) adhered onto the media while most separated into a powder. Attempting to coalesce this powder by melting resulted in ignition. To complete the ore-to-ingot process, the magnesium product was purified by vacuum distillation. The Mg distillate easily coalesced when melted. Vacuum distillation of the media and powder resulted in an overall Mg ore-to-ingot yield of 29.1 ± 0.5% for reduction at 1500 °C and 1550 °C. Vacuum distillation of only the powder resulted in an Mg ore-to-ingot yield of 18.5 ± 2.3% for reduction at 1400 °C and 1450 °C. The impurity profile of the magnesium ingot is listed in Table 3. The product Mg ingot was high in Ca, Na, and Ni but otherwise conformed to B92 standards [34]. Using stainless steel for reactor construction likely led to Ni contamination. The product purity could be improved by adding appropriate fluxes during melting and/or lowering the temperature of vacuum distillation. Handling the large amount of media with dilute Mg burdens the process, and an effective means of solids processing and Mg separation would be required for any large-scale operation.

4. Model development

4.1. Heat and mass transfer in the reduction reactor

Previous studies [26,35] revealed the kinetics of C/MgO pellets under idealized conditions. Extrapolation of those rates to the system herein predicted production rates of 250–600 g/h Mg. Given that the experimentally measured production rates were lower (12.5–115.1 g/h Mg), heat and mass transfer limitations existed within the reactor. The macroscopic species balance kinetic model [26] was integrated in a heat and mass transfer model of the reactor to reveal the key phenomena that govern $Mg_{(g)}$ production. Although many solid-state kinetic models are independent of pressure [36], the macroscopic species balance model takes into account the effect of CO and $Mg_{(g)}$ partial pressures on the reaction rate. This allows for mass transfer to influence the reactor performance.

The Navier-Stokes (NS) equations were discretized using the finite volume method and the method of lines [37] for a continuum solid (pellet) phase and gas phase inside the reduction furnace. The resulting set of ODEs was solved using the differential equation solver ODE15s in MATLAB. The axisymmetric problem was formulated for a 2D (r x z) grid. The solution converged for a grid size of 15 × 80 for the solid and gas phases inside of the tube and 5 × 80 for the tube. Eqs. (7)–(10) below describe the governing equations used for the heat and mass transfer within the reacting bed which were loosely based on the work of Z'graggen and Steinfeld [38].

$$(1-\varphi)\overline{\rho_s}\overline{Cp_s}\left(\frac{\partial \overline{T_s}}{\partial t} + \vec{v}_s\nabla\overline{T_s}\right) = \nabla\left(k_{r,eff}\nabla\overline{T_s}\right) - h_{g,s}A\Delta\overline{T_{g,s}} + \sum_n r_n{\cdot}\Delta H_{r_n} \tag{7}$$

$$\varphi\overline{\rho_g}\overline{Cp_g}\left(\frac{\partial \overline{T_g}}{\partial t} + \vec{v}_g\nabla\overline{T_g}\right) = h_{g,s}A\Delta\overline{T_{g,s}} + \sum_n\sum_i r_n{\cdot}H_i \tag{8}$$

$$\left(\frac{\partial \overline{C_i}}{\partial t} + \vec{v}_g\nabla\overline{C_i}\right) = \nabla\left(\mathfrak{D}_{i,j}\nabla\overline{C_i}\right) + \sum_n r_n \tag{9}$$

$$\overline{\rho_t}\overline{Cp_t}\frac{\partial \overline{T_t}}{\partial t} = \nabla\left(k_t\nabla\overline{T_t}\right) \tag{10}$$

The subscript 's' indicates the solid phase, 'g' the gas phase, 'i' the gaseous species, and 't' the tube. The reaction was assumed to occur in the solid phase, and hot product gases were introduced into the gas phase at the solid temperature. For the gas phase, the energy balance (Eq. (8)) included advection, gas-solid heat exchange, and hot gases production. The mass balance on the gas phase (Eq. (9)) included advection, diffusion, and reaction. For the solid phase, the concentration of solids (C and MgO) was assumed to be constant. As pellets shrunk from reaction, the mole fraction, pellet density, and packing fraction did not change significantly, so even though pellets reacted as they moved through the furnace, the concentration of solids at any point in space and time within the reaction tube remained constant. The energy balance on the solid phase (Eq. (7)) included conduction, advection, radiation, gas-solid heat exchange, and reaction. The optically thick bed was modeled by a diffusion approximation where the relative contributions of conduction and radiation to the effective thermal conductivity were calculated by Nusselt's correlation [39].

$$k_{r,eff} = \left(\frac{\varphi}{k_r} + \frac{(1-\varphi)}{k_{eff}}\right)^{-1} \tag{11}$$

Eq. (12) estimated the radiative contribution to thermal conductivity where the value of E equaled the pellet emissivity ($\epsilon = 0.7$) [40].

$$k_r = 4ED_{pellet}\sigma T^3 \tag{12}$$

The effective thermal conductivity (k_{eff}) measured by laser flash analysis (LFA) was $0.25\ W{\cdot}m^{-1}{\cdot}K^{-1}$.

Heat entered the reactor by conducting through the reaction tube (Eq. (10)). The external wall boundary of the tube was heated by convection [41] and radiation [42] from the furnace heaters.

The velocity of the gas phase was estimated by Darcy's law, where the permeability was fit ($\kappa = 2.07{\cdot}10^{-8}\ m^2$) to the experimentally measured pressure drop. As a first approximation, the composition of the gas inside a C/MgO pellet was assumed to be equal to the gas composition inside the bed (outside the pellet) because of the porous nature ($\varphi = 0.61 \pm 0.02$) of the pellets. This reduced the two levels of porosity (pellet and bed) to a single porous phase.

The velocity of the solid phase because of pellet gasification contributed to the solid phase energy balance. Many different methods exist [43–45] to calculate the solids velocity from bed gasification. Here only axial motion of the solids was considered, and pellets were assumed to follow a shrinking core mechanism, as was observed experimentally. The solids void fraction was assumed to be constant, and the flow of solids out of a cell was set equal to the gasification of solids

Table 3
Impurity profile of Mg ingot in ppm (balance Mg).

Al	Ca	Cu	Fe	Mn	Na	Ni	Ti	Zn
264	8766	5	283	4	223	80	105	34

Please cite this article as: B.A. Chubukov, S.C. Rowe, A.W. Palumbo, et al., Investigation of continuous carbothermal reduction of magnesia by magnesium vapor condensation onto ..., Powder Technol., https://doi.org/10.1016/j.powtec.2019.01.067

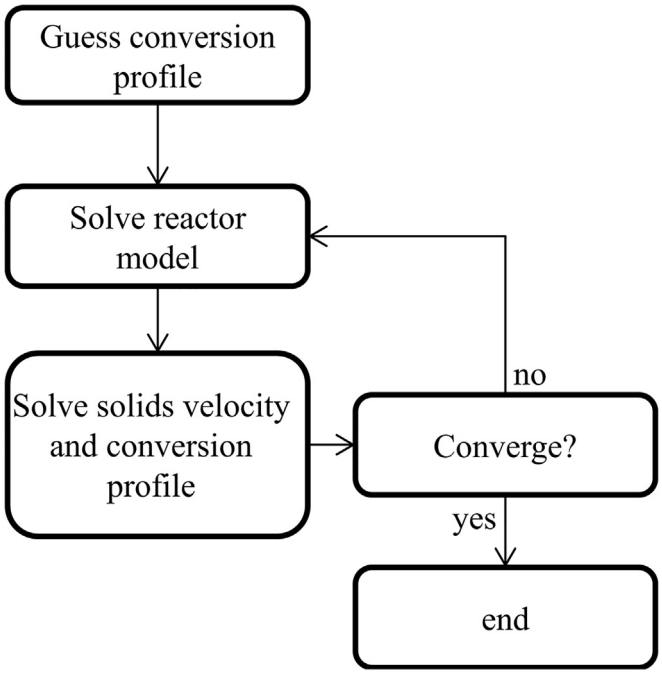

Fig. 7. Iterative loop for solving NS equations and solids flow profile.

from all cells below, Eq. (13),

$$\overrightarrow{v_{zi}} = \frac{\sum_{i=i+1}^{bot} \sum_n \left(r_{n_i} \cdot V_{cell}\right)}{C_{C/MgO} A_z} \tag{13}$$

where "*i*" counts the axial cells from top to bottom, and "*bot*" refers to the bottom cell. At the bottom of the bed, pellets gasified completely, and fresh pellets entered from the top. This velocity was calculated by an iterative loop separate from the NS equations, Fig. 7. In this loop, the solids velocity and C/MgO conversion in a pellet were calculated such that pellets gasified completely in the bottom cell.

4.2. Model results

Fig. 8 illustrates the model solution for a furnace temperature of 1400 °C. Solutions at higher temperatures showed a similar pattern only differing in magnitude. The SiC tube heated to nearly ($\Delta T_{tube\text{-}furnace}$ < 10 °C) the furnace temperature, and the gas heated to nearly the solids temperature ($\Delta T_{gas\text{-}solid}$ < 25 °C). The large heat sink from endothermic reaction created a radial temperature gradient within the bed, and the temperature at the centerline was 20–100 °C cooler than the furnace temperature. The reaction rate and product concentrations were greatest near the tube wall but resulted in a negligible radial pressure gradient because of the relatively narrow tube (L/D = 24). The concentration of product gases nearly reached equilibrium (>90%) in the majority of the bed, limiting the production rate. The top and bottom of the bed near the tube wall were furthest from equilibrium. At the top of the bed, dilution by argon sweep gas minimized product gas partial pressures. At the bottom of the bed, high gas velocities at low pressures effectively removed product gases. The reaction rate was fastest at these points even though the temperature was highest at the center (axial) of the hot-zone. Both mass and heat transfer limitations hindered the Mg production rate. As the temperature and reaction rate were highest near the tube wall, the solids velocities were fastest there because of rapid pellet gasification. Further, as the corners of the bed were furthest from equilibrium, a greater extent of conversion occurred in these areas. Even though all pellets reached complete conversion at the bottom of the bed, those pellet travelling near the tube wall converted more at the bottom of the bed than those travelling along the centerline. This resulted in a lower pellet conversion near the tube wall than at the centerline for a given axial position.

Fig. 9 shows the projected effect of increasing bed diameter on the production rate. The area-averaged Mg production rate is maximum around 16 $mg \cdot h^{-1} \cdot cm^{-2}$ at a diameter of 10 cm (L/D = 9.1). For larger bed diameters, the reactor production is limited completely by heat transfer. Minimizing bed diameter reduces the heat transfer limitations, resulting in the greatest volume averaged production rates. When indirectly heated, many small diameter reaction tubes will maximize Mg production. A wide and directly heated furnace may overcome these heat and mass transfer limitations.

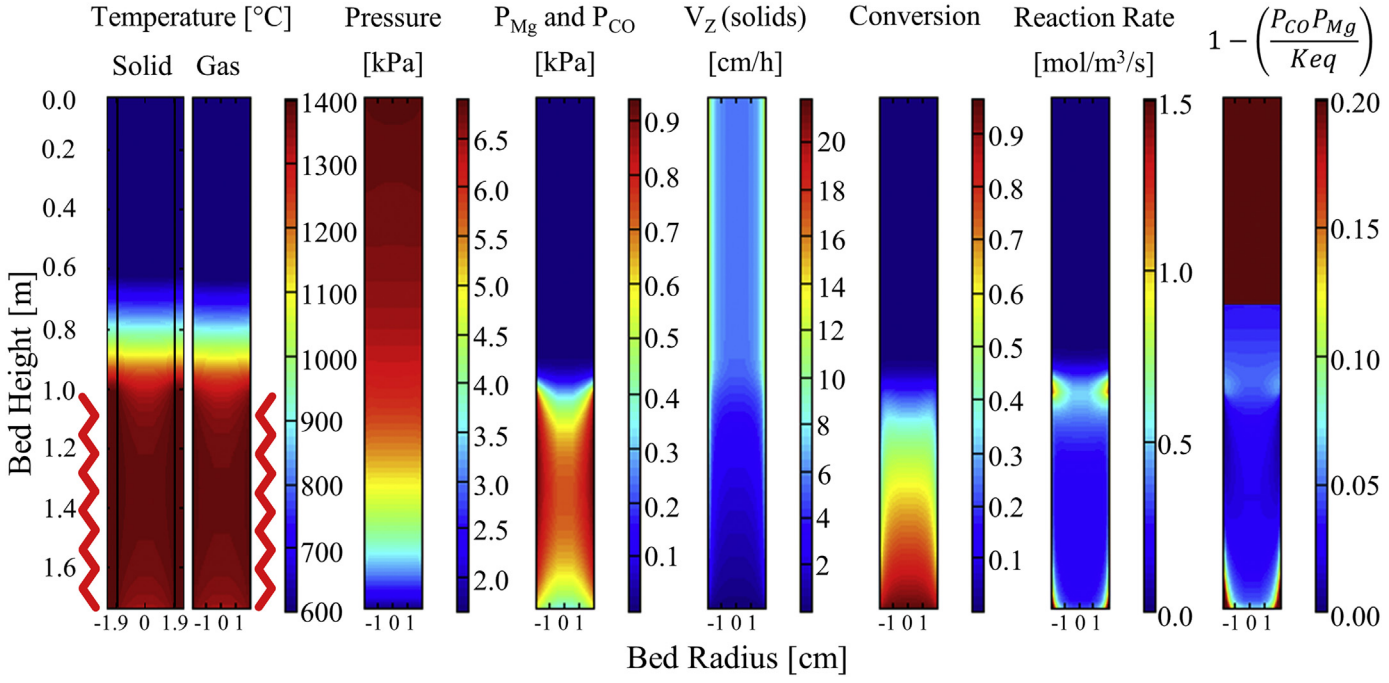

Fig. 8. Model results for a furnace temperature of 1400 °C.

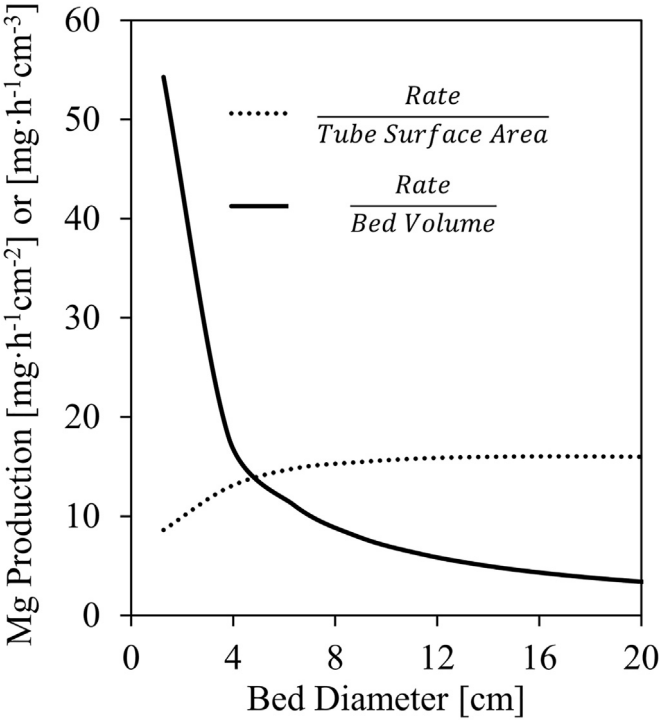

Fig. 9. Predicted magnesium production rates at a furnace temperature of 1400 °C for varying tube diameter.

5. Conclusion

The half-system artificially generated the products of MgO CTR by evaporating Mg and mixing with CO. Condensation of $Mg_{(g)}$ at a partial pressure of 0.5 kPa resulted in high yields (>85%) for $\dot{m}_{Mg} = 29.96 \pm 0.13$ g/h on carbide, oxide, and steel media. Steel media showed the greatest bed retention and ease of Mg separation. The condenser was scaled-up for use in the full-system in which MgO CTR between 1400 °C and 1550 °C resulted in $Mg_{(g)}$ production rates of 12.5–115.1 g/h. The reduction reactor operated continuously by feeding equimolar C/MgO pellets to replace those gasified within the bed. Initial operation resulted in high Mg yield (80%), but further reduction lowered yield. The accumulation of Mg and reversion products in the condenser promoted further reversion. The operating method proved to be feasible, but the initial condenser design did not result in stable operation. For successful operation, the condenser must be designed with a high surface area medium to promote heat and mass transfer, allowing for shorter gas and solid residence times. A finite volume model of the reduction reactor revealed heat and mass transfer limitations. Extrapolating the model predicted that the reactor throughput would be completely limited by heat transfer for bed diameters greater than ~10 cm. A wide and directly heated reduction furnace may overcome these limitations.

Declaration of interest

Boris Chubukov, Scott Rowe, and Aaron Palumbo are co-founders of Big Blue Technologies and are working to commercialize magnesium production by carbothermal reduction.

Nomenclature

CTR	Carbothermal reduction
SS	Stainless steel
OD	Outer diameter
ID	Inner diameter
slm	Standard liter/min
P_i	Partial pressure of "i"
Y_{hs}	Yield of $Mg_{(s)}$ from $Mg_{(g)}$ in half-system
Cp_i	Heat capacity of "i"
$T_{s,f}$	Outlet solids temperature
$T_{g,f}$	Outlet gas temperature
T_{frez}	Mg freezing temperature
$\dot{Q}$	Rate of heat absorbed by media
k_r	Radiant thermal conductivity
$k_{r,eff}$	Effective and radiant packed bed thermal conductivity
k_{eff}	Effective pellet thermal conducitivity
E	Exchange factor
σ	Stefan-Boltzmann constant
V_{cell}	Volume of cell
ρ	Density
$h_{g,s}$	Gas-solid heat transfer coefficient
$\mathfrak{D}_{i,j}$	Binary gas diffusivity
n_i	Moles of "i"
$\dot{n}_i$	Molar flow of "i"
R_B	Bed retention
m_i	Mass of "i"
$\dot{m}_i$	Mass flow of "i"
C_i	Bulk molar concentration of "i"
A_z	Cross sectional area
Y_{fs}	Yield of $Mg_{(s)}$ from $Mg_{(g)}$ in full-system
$\vec{v}$	Velocity
$T_{s,i}$	Inlet solids temperature
$T_{g,i}$	Inlet gas temperature
T_{cond}	Mg condensation temperature
A	Gas-solid interfacial area
U	Overall heat transfer coefficient
ΔT_{LM}	Log mean gas-solid temperature difference
ΔH_i	Enthalpy of reaction or phase change "i"
φ	Bed void fraction
D_{pellet}	Pellet diameter
r_n	Rate of reaction "n"
$\Delta T_{g,s}$	Gas-solid temperature difference
H_n	Enthalpy of gas product "n"

Acknowledgements

The authors acknowledge financial support from the National Science Foundation: Award 1622824 and from the Advanced Research Projects Agency-Energy (ARPA-E) of the US Department of Energy (DOE): Award AR0000404. We thank Dragan Mejic for fabricating all custom equipment used on both experimental systems.

References

[1] G. Brooks, S. Trang, P. Witt, M. Khan, M. Nagle, The carbothermic route to magnesium, JOM 58 (2006) 51–55.
[2] S. Ramakrishnan, P. Koltun, P. Warrandale, A comparison of the greenhouse impacts of magnesium produced by electrolytic and Pidgeon processes, Essent. Read. Magnes. Technol. (2004) 169–174.
[3] S. Das, Primary magnesium production costs for automotive applications, JOM 60 (2008) 63–69.
[4] R. Winand, M. Van Gysel, A. Fontana, L. Segers, J. Carlier, Production of magnesium by vacuum carbothermic reduction of calcined dolomite, Trans. Instn. Min. Metall (Sect. C) (1990) 105–111.
[5] F.J. Hansgirg, Thermal reduction of magnesium compounds, The Iron Age 18 (1943) 56–63.
[6] H.A. Doerner, Process for Producing Magnesium Metal, US2328202 1943.
[7] F.J. Hansgirg, Process of Magnesium Production, US2437815 1948.
[8] L.H. Prentice, M.W. Nagle, T.R. Barton, S. Tassios, B.T. Kuan, P.J. Witt, K.K. Constanti-Carey, Carbothermal Production of Magnesium: CSIRO's MagSonic™ 8482; Process, Magnesium Technol, 2012 29–35.
[9] H. Fumio, Method for Obtaining Mg and Ca through Carbon Reduction, US4147534 1979.
[10] J.S. Frederiksen, P. Saxby, J.R. Boulle, R.R. Odle, Method and Apparatus for Condensing Metal Vapours Using a Nozzle and a Molten Collector, US20120297930 2012.

Please cite this article as: B.A. Chubukov, S.C. Rowe, A.W. Palumbo, et al., Investigation of continuous carbothermal reduction of magnesia by magnesium vapor condensation onto ..., Powder Technol., https://doi.org/10.1016/j.powtec.2019.01.067

[11] T.J. Griswold, T.H. Mcconica, Method and Apparatus for Condensing Metallic Vapors, US2416992 1947.
[12] J.J.N. Reding, Apparatus for Condensation of a Metal Vapor, US3042511 1962.
[13] G. Bassereau, Process and Apparatus for the Vacuum Production of Magnesium, US2446403 1948.
[14] R.L. Player, R.J. Dry, Condensation of Metal Vapors in a Fluidized Bed and Apparatus, US5358548 1994.
[15] M.A. Julian, Process for Recovering Magnesium, EP0075836 A3 1985.
[16] T.J. Griswold, Recovery of Magnesium, US2381405 1945.
[17] D.S. Chisholm, Recovery of Magnesium from Vapor Mixtures, US2381403 1945.
[18] R. Suchy, Production of Magnesium, US2051913 1936.
[19] S. Walther, Condensation of Magnesium Vapors, US3505063 1970.
[20] C.-B. Yang, Y. Tian, T. Qu, B. Yang, B.-Q. Xu, Y.-N. Dai, Production of magnesium during carbothermal reduction of magnesium oxide by differential condensation of magnesium and alkali vapours, J. Magnesium Alloys 1 (2013) 323–329.
[21] M.H. Josefine, Production of Magnesium, US2582119 1952.
[22] T.H. Mcconica, Method of Producing Magnesium, US2391727 1945.
[23] R. Anderson, N. Parlee, Carbothermic reduction of refractory metals, J. Vac. Sci. Technol. 13 (1976) 526–529.
[24] K. Erdmann, Production of Metallic Magnesium, US2123990 1938.
[25] C.-B. Yang, Y. Tian, T. Qu, B. Yang, B.-Q. Xu, Y.-N. Dai, Magnesium vapor nucleation in phase transitions and condensation under vacuum conditions, Trans. Nonferrous Metals Soc. China 24 (2014) 561–569.
[26] B.A. Chubukov, A.W. Palumbo, S.C. Rowe, I. Hischier, A.J. Groehn, A.W. Weimer, Pressure dependent kinetics of magnesium oxide carbothermal reduction, Thermochim. Acta 636 (2016) 23–32.
[27] I. Hischier, B.A. Chubukov, M.A. Wallace, R.P. Fisher, A.W. Palumbo, S.C. Rowe, A.J. Groehn, A.W. Weimer, A novel experimental method to study metal vapor condensation/oxidation: Mg in CO and CO 2 at reduced pressures, Sol. Energy 139 (2016) 389–397.
[28] C.-B. Yang, Y. Tian, T. Qu, B. Yang, B.-Q. Xu, Y.-N. Dai, Analysis of the behavior of magnesium and CO vapor in the carbothermic reduction of magnesia in a vacuum, J. Magnesium Alloys 2 (2014) 50–58.
[29] B.A. Chubukov, A.W. Palumbo, S.C. Rowe, M.A. Wallace, A.W. Weimer, Enhancing the rate of magnesium oxide carbothermal reduction by catalysis, milling, and vacuum operation, Ind. Eng. Chem. Res. 56 (2017) 13602–13609.
[30] E.Y. Shafirovich, U. Goldshleger, Combustion of magnesium particles in CO2/CO mixtures, Combust. Sci. Technol. 84 (1992) 33–43.
[31] W. Shi, M. Kobashi, T. Choh, Wetting of alumina, iron and stainless steel substrates by molten magnesium, Zeitschrift Fur Metallkunde 92 (2001) 382–385.
[32] D. Zhang, P. Shen, L. Shi, Q. Lin, Q. Jiang, Wetting and evaporation behaviors of molten Mg on partially oxidized SiC substrates, Appl. Surf. Sci. 256 (2010) 7043–7047.
[33] A. Weidenkaff, A. Reller, A. Wokaun, A. Steinfeld, Thermogravimetric analysis of the ZnO/Zn water splitting cycle, Thermochim. Acta 359 (2000) 69–75.
[34] A. International, Standard Specification for Unalloyed Magnesium Ingot and Stick for Remelting2017.
[35] B.A. Chubukov, A.W. Palumbo, S.C. Rowe, M.A. Wallace, A.W. Weimer, Enhancing the rate of magnesium oxide carbothermal reduction by catalysis, milling, and vacuum operation, Ind. Eng. Chem. Res. 56 (46) (2017) 13602–13609.
[36] A. Khawam, D.R. Flanagan, Solid-state kinetic models: basics and mathematical fundamentals, J. Phys. Chem. B 110 (2006) 17315–17328.
[37] S. Hamdi, W.E. Schiesser, G.W. Griffiths, Method of lines, Scholarpedia 2 (2007) 2859.
[38] A. Z'graggen, A. Steinfeld, A two-phase reactor model for the steam-gasification of carbonaceous materials under concentrated thermal radiation, Chem. Eng. Process. Process Intensif. 47 (2008) 655–662.
[39] W. Nusselt, Die Übertragung der Wärme bei der Bone-Schnabel-Feuerung, Zs. d. Bayr. Revis, Vereins 17 (1913) 125.
[40] W. Schotte, Thermal conductivity of packed beds, AICHE J. 6 (1960) 63–67.
[41] S. Whitaker, Forced convection heat transfer correlations for flow in pipes, past flat plates, single cylinders, single spheres, and for flow in packed beds and tube bundles, AICHE J. 18 (1972) 361–371.
[42] R.B. Bird, W.E. Stewart, E.N. Lightfoot, Transport Phenomena, John Wiley & Sons, 2007.
[43] J. Cooper, W. Hallett, A numerical model for packed-bed combustion of char particles, Chem. Eng. Sci. 55 (2000) 4451–4460.
[44] M. Gómez, J. Porteiro, D. Patiño, J. Míguez, CFD modelling of thermal conversion and packed bed compaction in biomass combustion, Fuel 117 (2014) 716–732.
[45] S. Hermansson, H. Thunman, CFD modelling of bed shrinkage and channelling in fixed-bed combustion, Combust. Flame 158 (2011) 988–999.

Please cite this article as: B.A. Chubukov, S.C. Rowe, A.W. Palumbo, et al., Investigation of continuous carbothermal reduction of magnesia by magnesium vapor condensation onto ..., Powder Technol., https://doi.org/10.1016/j.powtec.2019.01.067